Electronic states of moiré modulated Cu films

2012 J. Phys.: Condens. Matter 24 335502

(http://iopscience.iop.org/0953-8984/24/33/335502)

J. Phys.: Condens. Matter **24** (2012) 335502 (7pp) doi:10.1088/0953-8984/24/33/335502

Electronic states of moiré modulated Cu films

P Moras[1], P M Sheverdyaeva[1], C Carbone[1], D Topwal[2], L Ferrari[3], G Bihlmayer[4], S Ouazi[5], S Rusponi[5], A Lehnert[5] and H Brune[5]

[1] Istituto di Struttura della Materia, Consiglio Nazionale delle Ricerche, Trieste, Italy
[2] International Center for Theoretical Physics (ICTP), I-34014 Trieste, Italy
[3] Istituto dei Sistemi Complessi, Consiglio Nazionale delle Ricerche, Roma, Italy
[4] Peter Grünberg Institut and Institute for Advanced Simulation, Forschungszentrum Jülich and JARA, DE-52425 Jülich, Germany
[5] Institute of Condensed Matter Physics, Ecole Polytechnique Fédérale de Lausanne (EPFL), Station 3, CH-1015 Lausanne, Switzerland

E-mail: paolo.moras@trieste.ism.cnr.it

Received 21 May 2012, in final form 4 July 2012
Published 20 July 2012
Online at stacks.iop.org/JPhysCM/24/335502

Abstract
We examined by low-energy electron diffraction and scanning tunneling microscopy the surface of thin Cu films on Pt(111). The Cu/Pt lattice mismatch induces a moiré modulation for films from 3 to about 10 ML thickness. We used angle-resolved photoemission spectroscopy to examine the effects of this structural modulation on the electronic states of the system. A series of hexagonal- and trigonal-like constant energy contours is found in the proximity of the Cu(111) zone boundaries. These electronic patterns are generated by Cu sp-quantum well state replicas, originating from multiple points of the reciprocal lattice associated with the moiré superstructure. Layer-dependent strain relaxation and hybridization with the substrate bands concur to determine the dispersion and energy position of the Cu Shockley surface state.

Lattice size and symmetry of the crystalline substrate influence deeply the growth properties and electronic states of hetero-epitaxial thin films. The lattice mismatch across the interface plane can alter sizably the in-plane parameters of the overlayer material, thus modifying the electronic band structure of the system. This mechanism is well known in semiconductor physics and exploited to tailor the electronic and optical properties of hetero-junctions and multilayers [1]. Strained hetero-structures are widely used as active components in several types of devices, such as quantum well (QW) lasers [2], field effect transistors [3], light emitting diodes [4] and photo-detectors [5]. The scenario is different for thin metal films. Metallic bonds favor the strain relief within the first few atomic layers from the interface, often through the formation of domain walls [6], dislocation patterns [7–11] and long-range moiré modulations [9, 11–14]. As a consequence, the lattice mismatch gives rise to relevant effects in the band structure of a metal film on a much shorter length scale than in semiconductors.

Band features ascribed to substrate-induced structural modulations could be observed in some sp-metal film systems by surface sensitive techniques, such as scanning tunneling spectroscopy (STS) and angle-resolved photoemission spectroscopy (ARPES). For instance, the Shockley surface state of 1 and 2 ML (monolayer) Cu films on Ru(0001) lies entirely above the Fermi level (E_F) [15], at variance with Cu(111) bulk crystals [16]. This energy shift, which reduces as the film thickness increases, is linked to the layer-dependent release of the interface tensile strain. The Shockley surface state of Ag films on Si(111) shows a similar behavior [17]. The triangular dislocation network [18] and moiré-like superstructure [12, 19] of 1 ML Ag on Cu(111) give rise to characteristic surface state gaps. The QW state formation is inhibited within specific thickness regimes by substrate-induced deformations of the In and Pb film structures on Si(100) [20]. A direct relation between in-plane lattice strain and large QW state effective mass exists in Pb films on Si(111) [21]. One-dimensionally modulated Ag films on In-modified Si(111) [22] and GaAs(110) [23] display anisotropic QW dispersions near the surface Brillouin zone center. In this context, thin metal films, where substrate-induced structural modulation extends

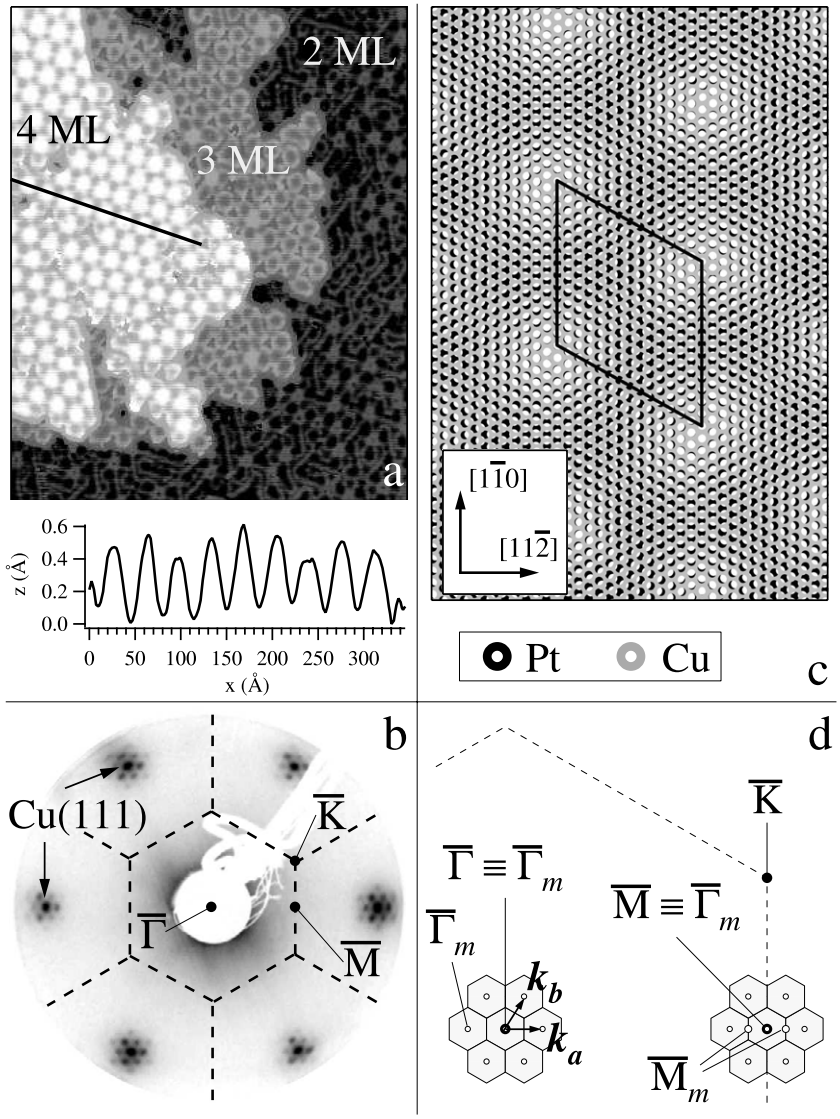

Figure 1. (a) Constant current STM image for a 3 ML Cu film deposited on Pt(111) at room temperature. The line profile is measured along the [1$\bar{1}$0] substrate direction on the 4 ML high terrace. (b) LEED pattern for a 5 ML Cu film grown on Pt(111) at 140 K and annealed to room temperature. The principal Cu(111) spots are surrounded by the moiré-related spot replicas that display a clear three-fold symmetry. (c) Real space ball model showing the registry relation between the Cu(14 × 14) and Pt(13 × 13) supercells. The high-symmetry directions are shown. (d) Surface Brillouin zones and symmetry points of a bulk-truncated Cu(111) crystal and a moiré-modulated Cu film on Pt(111).

to several atomic layers from the interface to the surface, represent an interesting and so far not much explored case.

In a nanometer thick metal film the electron confinement effects along the direction perpendicular to the surface give rise to discrete electronic states delocalized over the entire film thickness. Substrate-induced modulations involving the whole structure of a thin film are expected to influence the properties of these QW states. The present paper reports an investigation of thin Cu films grown on Pt(111). Scanning tunneling microscopy (STM) and low-energy electron diffraction (LEED) analysis reveals the formation of a large moiré supercell from 3 to about 10 ML Cu. The electronic structure of the system near E_F is probed by ARPES and displays a series of hexagonal- and trigonal-like constant energy contours. These patterns derive from Cu sp QW state replicas, centered at the $\bar{\Gamma}$ points of adjacent moiré-related surface Brillouin zones. Energy position and band dispersion of the Cu Shockley surface state appear to be determined by hybridization with the substrate states and thickness dependent attenuation of the structural modulation.

The Pt(111) single crystal was prepared by cycles of Ar ion sputtering at 300 K, exposure to oxygen at 850 K and flash to 1100 K. STM measurements were taken in a dedicated UHV chamber in Lausanne. Cu films with multiple exposed layers were obtained by room temperature deposition, to allow calibration of the local coverage and detailed characterization of the layer-dependent surface morphology (figure 1(a)). LEED and ARPES analysis was carried out at the VUV photoemission beamline (Elettra, Trieste) on 3–12 ML Cu films grown at 140 K and annealed to room temperature ('two-step' growth [24]). This procedure results in single height Cu layers over macroscopic areas of the sample. The ARPES data were measured at 70 and 165 eV photon energy with the sample at room temperature. Constant

energy cuts were constructed from sets of photoemission intensity maps acquired within an azimuthal sector of 60° covering the angle between subsequent $\bar{\Gamma}$–$\bar{M}$ surface axes. First-principles electronic structure calculations for a free-standing 5 ML Cu film with the bulk lattice constant were performed using density functional theory in the local density approximation [25] as implemented in the FLEUR code [26].

Figure 1 reports the results of structural investigations for thin Cu films on Pt(111). The STM constant current mode image of figure 1(a) shows the morphology of a 3 ML Cu film deposited at room temperature. Three terraces with heights of 2, 3 and 4 ML and separated by atomic steps are simultaneously observed[6]. The layer-dependent strain relaxation of the lattice misfit between Pt and Cu ($(a_{Cu} - a_{Pt})/a_{Pt} = -7.9\%$, with $a_{Pt} = 3.92$ Å, $a_{Cu} = 3.61$ Å) gives rise to different Cu(111)-based surface morphologies. The first Cu ML (not shown in figure 1(a)) grows pseudomorphic to the substrate [27]. On the second ML Cu atoms assemble in two energetically equivalent structures, characterized by a labyrinth-like motif and a trigonal network of partial surface dislocations [28] that coexist on the 2 ML terrace. A long-range moiré modulation develops on the 4 ML high terrace. The symmetry axes of this superstructure parallel those of the substrate. The line profile below figure 1(a), acquired along the Pt[$1\bar{1}0$] direction, indicates a corrugation of 0.4 Å and a periodicity of 35 ± 2 Å, which corresponds to 12.6 ± 0.7 Pt atoms or 13.7 ± 0.7 Cu atoms[7]. The moiré superstructure persists up to about 10 ML, with a corrugation that decreases as the film thickness increases. A similar but less ordered reconstruction is observed also on the 3 ML terrace.

The LEED pattern of a uniformly thick 5 ML Cu film is displayed in figure 1(b). Arrows indicate the principal Cu spots, whose positions, evaluated by comparison with the substrate diffraction pattern, coincide with those of a bulk-truncated Cu(111) crystal. Sharpness and intensity of the moiré-induced extra-spots are maximal for 5 ML, fade away monotonously with increasing coverage and vanish at 12 ML. For all investigated films the diffraction patterns have three-fold symmetry and unit vectors collinear to those of the 1 × 1 Pt cell. The reciprocal distance between the moiré-related spots (0.202 ± 0.011 Å^{-1}), compared to the separation between the substrate spots (2.618 Å^{-1}) or the principal Cu spots (2.842 Å^{-1}), indicates that the period of the moiré supercell consists of 13.0 ± 0.7 Pt atoms or 14.0 ± 0.7 Cu atoms.

The best agreement between the STM and LEED results is given by a (13 × 13) substrate supercell with (14 × 14) adsorbed Cu atoms, which reduces the strain resulting from the lattice mismatch to only 0.8%. A model of this structure, displaying the registry relation between film and substrate, is shown in figure 1(c). Since the present paper focuses on the moiré-modulated electronic states of the Cu films, it is convenient to describe the system by means of the (14 × 14) Cu supercell, rather than referring to the substrate supercell. Figure 1(d) shows the Cu(111) and moiré-related surface Brillouin zones derived from the LEED images. The $\bar{\Gamma}$–$\bar{M}$ and $\bar{\Gamma}$–$\bar{K}$ reciprocal distances correspond to the Cu(111) bulk-derived values 1.421 Å^{-1} and 1.641 Å^{-1}, respectively, while the mini-Brillouin zone, whose symmetry points are identified by the subscript m, has unit vectors $\boldsymbol{k}_a = (0.203\ \text{Å}^{-1}, 0)$ and $\boldsymbol{k}_b = (0.102\ \text{Å}^{-1}, 0.176\ \text{Å}^{-1})$. The mini-Brillouin zone is replicated around $\bar{M}$ in order to show the sequence of symmetry points along the $\bar{\Gamma}$–$\bar{M}$ direction.

Figure 2(a) displays the experimental Fermi surface map for the 5 ML Cu film along with boundaries (white dashed line) and high-symmetry points of the Cu(111) surface Brillouin zone. The data set was acquired at 165 eV photon energy, close to the Pt 5d Cooper minimum [29], to suppress the substrate emission and enhance the sensitivity to the Cu sp signal. The region around the $\bar{\Gamma}$ point is featureless, while a series of hexagonal- and trigonal-like photoemission band patterns are detected near and across the zone boundaries. A close-up of the experimental data for positive (k_x, k_y) values (figure 2(b)) shows in detail the constant energy contours of the system at E_F.

In order to understand the origin of the observed photoemission pattern, we performed *ab initio* electronic structure calculations for a free-standing 5 ML Cu(111) film. The Fermi surface of this system (figure 2(c)) consists in the Shockley surface state ring and five sp-derived QW contours (labeled with the band index n). The $n = 4, 5$ states are characterized by hexagonal- and trigonal-like shapes, respectively. Replicas of these two states, translated by moiré-related reciprocal vectors $\boldsymbol{k}_\parallel = i\boldsymbol{k}_a + j\boldsymbol{k}_b$ ($i, j = -1, 0, +1$, except $i = j = \pm 1$), are reported in figure 2(d) for positive (k_x, k_y) values. Every QW contour can be univocally identified with the notation $n_{i,j}$.

Besides matrix element (intensity) effects, figure 2(d) describes reasonably well the map of figure 2(b). Each portion of the photoemission pattern can be viewed as a sum of different $n = 4, 5$ state replicas. For instance, the three straight segments surrounding $\bar{K}$ derive from the overlap of two trigonal-like contours, namely $5_{1,-1} + 5_{0,-1}$, $5_{1,0} + 5_{0,1}$ and $5_{-1,0} + 5_{-1,1}$. Similarly, the band pairs $5_{-1,0} + 5_{0,-1}$ and $4_{-1,0} + 4_{0,-1}$ generate parts of the energy contours at smaller (k_x, k_y) values.

Figure 3(a) shows a photoemission intensity map for the 5 ML Cu film, where several QW bands, with sp-like energy–momentum dispersion, are observed along the $\bar{\Gamma}$–$\bar{M}$ axis. The link between these states and the Fermi energy contours of figure 2(d) is given in figure 3(b) using the notation $n_{i,j}$. This band diagram, based on a fit to the experimental data, emphasizes the symmetric state distribution with respect to $\bar{M}$. Squares, diamonds and dots, whose size mimics the intensity of the corresponding photoemission signal in figure 3(a), refer to the $n = 3, 4, 5$ states, respectively. Notably, hybridization gaps of about 140 meV open between the $5_{0,0}$ band and its two replicas

[6] The Cu coverage calibration was performed by incremental depositions of small (∼0.1 ML) Cu amounts. The formation of the second ML was detected by the nucleation of new islands, displaying characteristic surface superstructures, on top of the first completed pseudomorphic ML [27].

[7] The nearest neighbor distances in Pt(111) and Cu(111) planes are 2.77 Å and 2.55 Å, respectively.

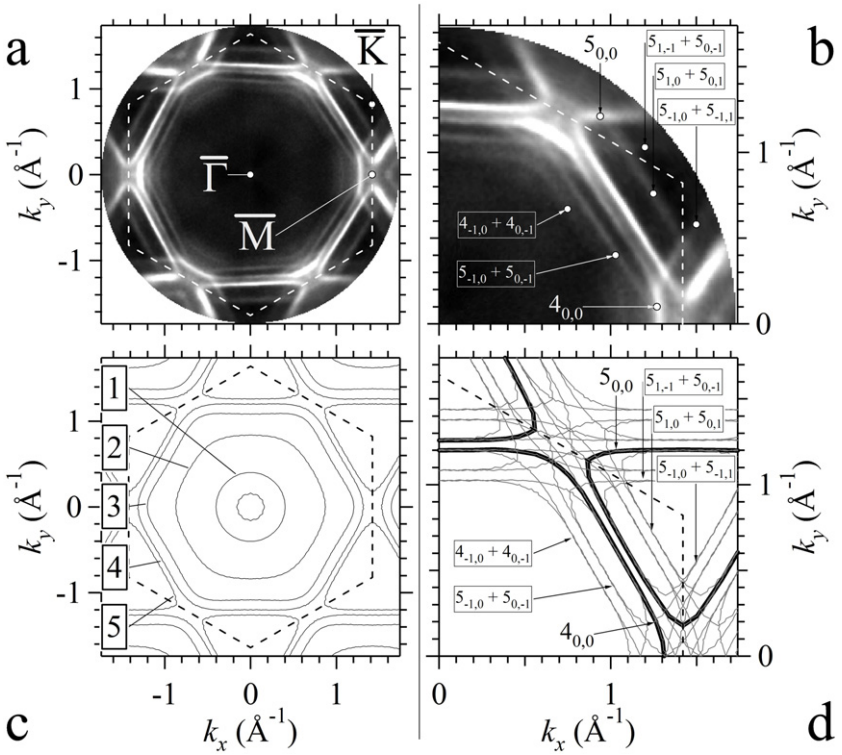

Figure 2. (a) Experimental Fermi surface for a 5 ML Cu film on Pt(111) measured at 165 eV photon energy. (b) Zoom of panel (a) for positive (k_x, k_y) values. (c) Calculated Fermi surface for a free-standing 5 ML Cu(111) film. The innermost circle is the Shockley surface state. The contours labeled $n = 1, \ldots, 5$ are the sp-derived QW states. (d) Band pattern generated by replicas of the $n = 4, 5$ QW contours shifted by moiré-related reciprocal lattice vectors (see text).

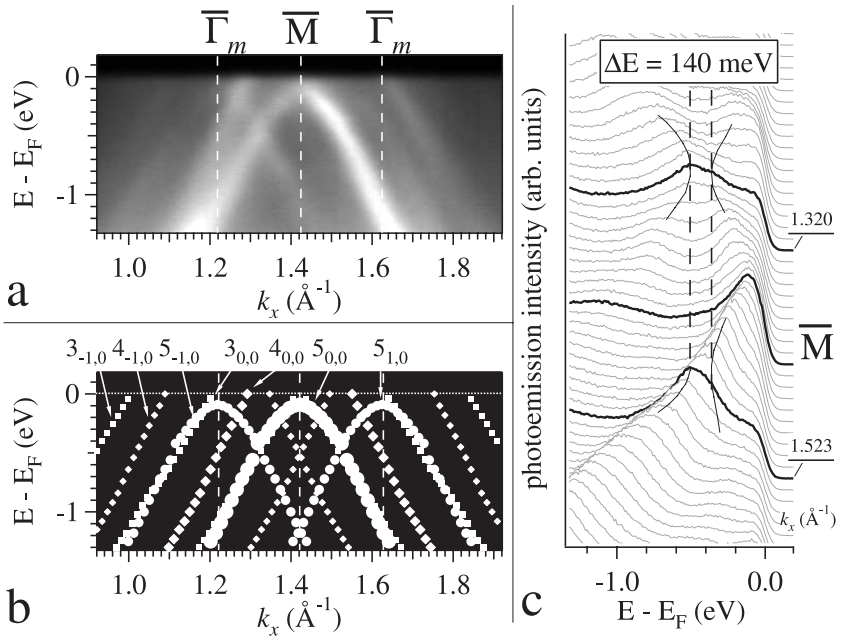

Figure 3. (a) Photoemission intensity map for a 5 ML Cu film on Pt(111) measured at 165 eV photon energy along the $\bar{\Gamma}$–$\bar{M}$ axis. (b) Band diagram derived from a fitting to the data of panel (a). Squares, diamonds and dots refer to the $n = 3, 4, 5$ states, respectively. (c) Set of photoemission spectra derived from panel (a). Thin continuous lines across the spectra help to identify the gap edges. The gaps are not fully resolved due to the finite width of the photoemission peaks.

$5_{-1,0}$ and $5_{1,0}$. Figure 3(c) reports photoemission spectra derived from figure 3(a), where the gap size can be directly evaluated. Thick lines identify spectra measured at the $\bar{M}$ ($\equiv\bar{\Gamma}_m$) point and at the mini-zone boundaries ($\bar{M}_m$) located at $k_x = 1.320$ and 1.523 Å^{-1} (see figure 1(d)). The observation of energy gaps that modify sizably the sp-like QW dispersion

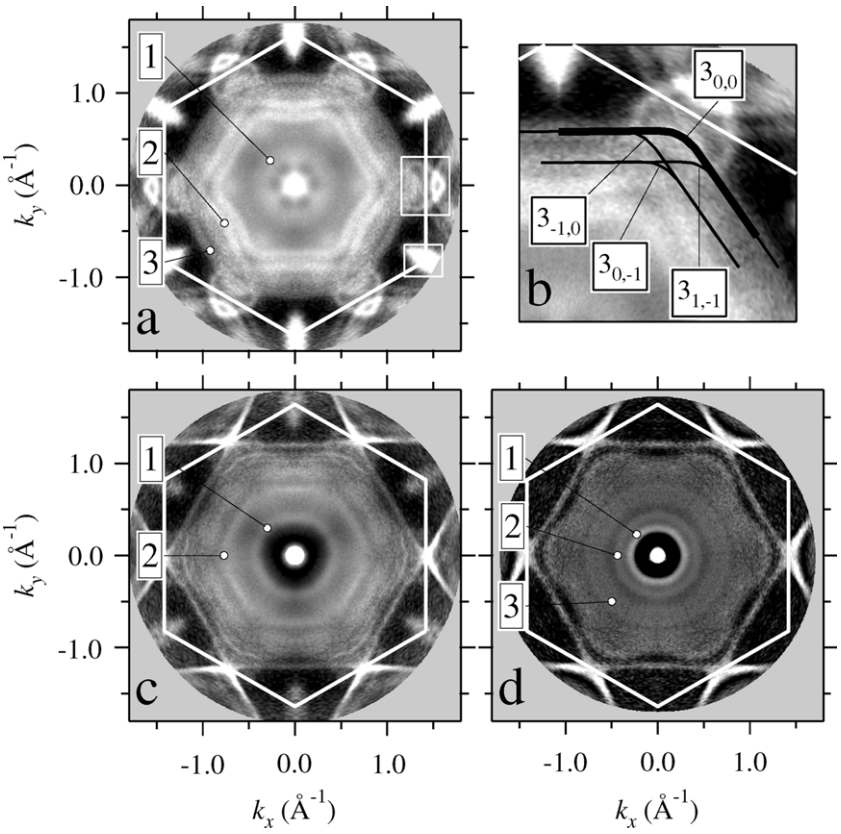

Figure 4. Constant energy photoemission intensity maps measured with 70 eV photons at 0.4 eV below E_F for ((a), (b)) 3, (c) 7, and (d) 12 ML Cu films on Pt(111). Substrate related features are enclosed in white boxes in panel (a). Thick and thin black lines are used in panel (b) to describe the moiré-induced pattern generated by the $n = 3$ QW state.

only in the vicinity of the Bragg planes suggests that the moiré-related potential represents a weak perturbation to the film electronic structure [30].

The thickness dependent structural changes pointed out by the LEED and STM analysis have a counterpart in the film electronic structure that can be followed by angle-resolved photoemission. Figure 4 reports constant energy cuts of the photoemission signal for ((a), (b)) 3, (c) 7 and (d) 12 ML Cu films at 0.4 eV below E_F. The data were acquired at 70 eV photon energy to enhance the sensitivity to Cu states near $\bar{\Gamma}$, at the cost of a non-negligible Pt emission for the thinnest Cu layer. The substrate bands give rise to oval and trigonal features (enclosed in rectangular boxes in panel (a)) near the $\bar{K}$ and $\bar{M}$ points, respectively, and spots halfway between the $\bar{\Gamma}$ and $\bar{M}$ points, that fade away monotonously with increasing Cu coverage.

Due to matrix element effects, the features observed in figure 4(a) differ markedly from those of figure 2(a). Near the zone center Cu and Pt states are expected to couple strongly, as shown for the closely related Ag/Pt(111) system [31]. In particular, the hybridization is responsible for the broad surface and $n = 1$ QW states energy contours. At larger wavevectors the effects of hybridization are attenuated and moiré-related state replicas can be identified. The outermost pair of hexagonal-like contours appears to be generated by in-plane translations of the $n = 3$ QW state according to the periodicity of the moiré superstructure. As an example, the $3_{0,0}$ state (thick line) and its $3_{-1,0}$, $3_{0,-1}$ and $3_{1,-1}$ replicas (thin lines) in figure 4(b) describe the formation of the photoemission pattern in figure 4(a). Analogously, the $n = 2$ QW states replicas account for the innermost pair of hexagonal-like contours of figure 4(a).

The effects of the moiré perturbation on the film electronic structure become weaker in the 7 ML data and undetectable at 12 ML. Besides the Shockley surface states, only the $n = 1, 2, 3$ QW rings can be resolved in the 12 ML data (figure 4(d)). The closer spacing between the QW states does not allow us to identify other bands at larger wavevectors. The convolution of unresolved QW contours gives rise to a flower-like pattern, whose concave shape is probably due to the hybridization with the substrate. Also the outermost hexagonal-like contour can be attributed to the accumulation of QW states near the zone boundaries.

The 7 ML Cu film (figure 4(c)) represents an intermediate case. The QW contours near the zone boundaries show the onset of the flower-like pattern formation observed at higher coverage. Although individual replicas are not resolved, the hexagonal-like shape of the $n = 2$ QW state and of the states closer to the zone boundary recalls the pattern generated by the moiré potential in the thinner film. In conclusion, the replicas associated with the moiré modulation are visible at least up to 7 ML, but disappear below 12 ML, in agreement with the results of the morphological analysis.

As mentioned above, also the properties of the sp-like Shockley surface states appear to be influenced by the

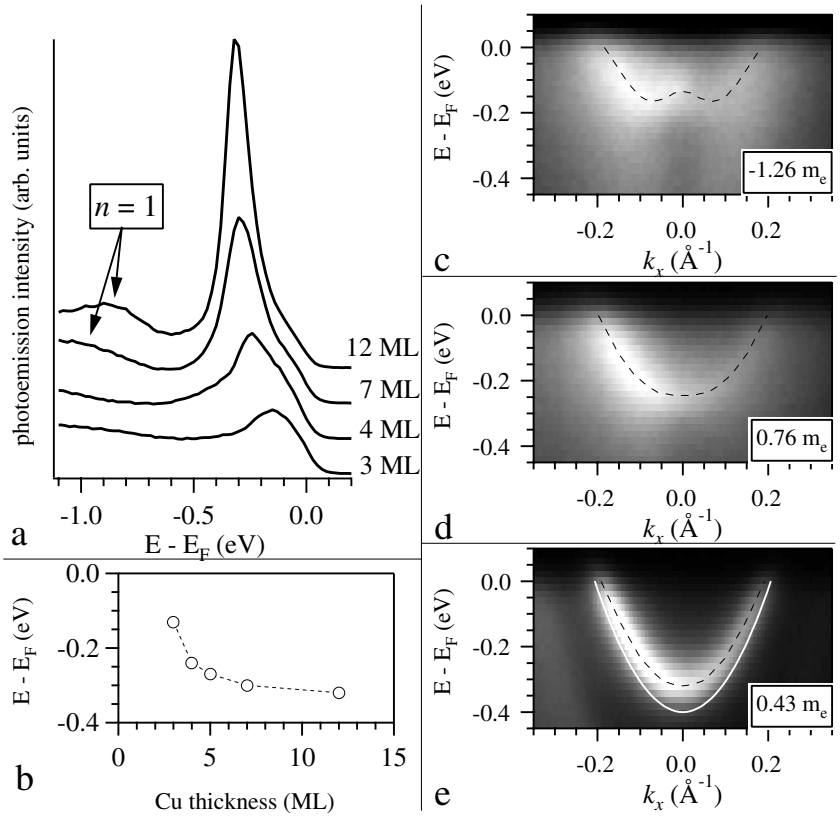

Figure 5. (a) Photoemission spectra acquired with 70 eV photons in normal emission geometry for Cu films of different thickness. The most intense feature is identified with the Cu(111) Shockley surface state. (b) Energy position of the surface state as a function of the film thickness. (c)–(e) Photoemission intensity maps of the Cu surface states measured along the $\bar{\Gamma}$–$\bar{\mathrm{M}}$ axis for (c) 3 ML, (d) 4 ML and (e) 12 ML Cu films. Dashed lines highlight the experimental band dispersion. The effective mass of the surface state is reported in each panel. The white line in panel (e) represents the surface band dispersion measured on a Cu(111) bulk crystal (from [16]) and shifted upwards in energy to account for the effects of temperature [33].

substrate. Figure 5(a) presents angle-resolved photoemission spectra taken at the $\bar{\Gamma}$ point of the Cu/Pt system for different Cu coverages (photon energy 70 eV). The surface state peak shifts continuously towards higher binding energies with increasing the film thickness (figure 5(b)). A similar observation by STS on the Shockley surface states of Cu films on Ru(0001) was mainly attributed to the release of the interface tensile strain that manifests itself with characteristic surface reconstructions [15]. In a simple model, the surface state behavior in the Cu/Pt system could be fully ascribed to the film strain induced by the lattice mismatch. For very thin films the Cu lattice expansion reduces the wavefunction overlap and, correspondingly, narrows the surface bandwidth. Since the centroid of this band lays above E_{F}, the surface state shifts upward in energy with respect to its position in unstrained Cu(111) crystals. As the film thickness increases, the structural distortions in the topmost Cu layers attenuate and, correspondingly, the energy shift decreases (see the discussion on the surface properties of the Ag/Cu(111) system in [32]).

However, the photoemission intensity maps for 3 and 4 ML Cu films in figures 5(c) and (d) suggest that hybridization effects concur to determine the surface state behavior, as indicated by the analysis of the surface band dispersion. For 3 ML the surface band displays a negative effective mass around $\bar{\Gamma}$ ($-1.26 \pm 0.24\ m_{\mathrm{e}}$, where m_{e} is the rest mass of a free electron), in contrast with its nearly free electron-like character at larger wavevectors. A surface state tail extending towards deeper binding energies generates the broad spot centered at $\bar{\Gamma}$ in figure 4(a). At 4 ML the effective mass turns positive ($0.76 \pm 0.15\ m_{\mathrm{e}}$), but the band bottom remains much flatter than that of a bulk Cu(111) crystal ($0.41\ m_{\mathrm{e}}$ [16]). All these features, whose origin was described in detail for the closely related case of Ag films on Pt(111) [31], highlight the role of hybridization between the Cu surface states and Pt substrate. The surface state wavefunction can couple in the proximity of $\bar{\Gamma}$ to Pt bulk bands with the same Λ_1 symmetry and opposite in-plane dispersion. At 3 and 4 ML the Cu surface state is sufficiently extended within the film to strongly hybridize with the substrate. The resulting flattening of the surface band bottom (figures 5(c) and (d)) adds to the upward energy shift, due to the layer-dependent interface tensile strain. At 12 ML (figure 5(e)) the surface wavefunction is decoupled from the substrate. The surface state has an effective mass of $0.43 \pm 0.08\ m_{\mathrm{e}}$ and parallels the dispersion measured on a bulk Cu(111) crystal (white line) [16, 33]. The residual energy shift may be ascribed to strain that persists below the topmost surface layers.

In conclusion, STM, LEED and photoemission studies reveal characteristic elements of the moiré-modulated

Cu/Pt(111) system, such as the supercell registry with the substrate. The slow attenuation of the moiré modulation as a function of the film thickness permits a direct inspection of the QW state behavior under the effects of a weak perturbation. The observed electronic patterns can be described in terms of QW state replicas following the moiré periodicity determined by STM. The surface state properties appear to be determined by the combined effects of lattice strain and direct wavefunction coupling to the substrate states.

Acknowledgment

We gratefully acknowledge support from the Italian MIUR (Grant No. PRIN 20087NX9YT).

References

[1] Lamberti C 2004 *Surf. Sci. Rep.* **53** 1 and references therein
[2] Kroemer H 2001 *Rev. Mod. Phys.* **73** 783 and references therein
[3] Drummond T J, Zipperian T E, Fritz I J, Schirber J E and Plut T A 1986 *Appl. Phys. Lett.* **49** 461
Zipperian T E, Dawson L R, Drummond T J, Schirber J E and Plut T A 1988 *Appl. Phys. Lett.* **52** 975
[4] Pullin M J, Hardaway H R, Heber J D, Phillips C C, Yuen W T, Stradling R A and Moeck P 1999 *Appl. Phys. Lett.* **74** 2384
[5] Brennanm K F and Haralson J 2000 *Superlatt. Microstruct.* **28** 77
[6] Brune H, Röder H, Boragno C and Kern K 1994 *Phys. Rev.* B **49** 2997
[7] Pötschke G O and Behm R J 1991 *Phys. Rev.* B **44** 1442
de la Figuera J, Schmid A K, Bartelt N C, Pohl K and Hwang R Q 2001 *Phys. Rev.* B **63** 165431
[8] Hamilton J C, Stumpf R, Bromann K, Giovannini M, Kern K and Brune H 1999 *Phys. Rev. Lett.* **82** 4488
[9] Lundgren E, Stanka B, Schmid M and Varga P 2000 *Phys. Rev.* B **62** 2843
[10] Ling W L, de la Figuera J, Bartelt N C, Hwang R Q, Schmid A K, Thayer G E and Hamilton J C 2004 *Phys. Rev. Lett.* **92** 116102
[11] Ling W L, Hamilton J C, Thürmer K, Thayer G E, de la Figuera J, Hwang R Q, Carter C B, Bartelt N C and McCarty K F 2006 *Surf. Sci.* **600** 1735
[12] Schiller F, Cordón J, Vyalikh D, Rubio A and Ortega J E 2005 *Phys. Rev. Lett.* **94** 016103
[13] Grioni M, Ast Ch R, Pacilé D, Papagno M, Berger H and Perfetti L 2005 *New J. Phys.* **7** 106
[14] Yuhara J, Schmid M and Varga P 2003 *Phys. Rev.* B **67** 195407
[15] Calleja F, García-Suárez V M, Hinarejos J J, Ferrer J, Vázquez de Parga A L and Miranda R 2005 *Phys. Rev.* B **71** 125412
[16] Reinert F, Nicolay G, Schmidt S, Ehm D and Hüfner S 2001 *Phys. Rev.* B **63** 115415
[17] Sawa K, Aoki Y and Hirayama H 2009 *Phys. Rev.* B **80** 035428
[18] Malterre D, Kierren B, Fagot-Revurat Y, Didiot C, García de Abajo F J, Schiller F, Cordón J and Ortega J E 2011 *New J. Phys.* **13** 013026
Abd El-Fattah Z M, Matena M, Corso M, García de Abajo F J, Schiller F and Ortega J E 2011 *Phys. Rev. Lett.* **107** 066803
[19] Bendounan A, Forster F, Ziroff J, Schmitt F and Reinert F 2005 *Phys. Rev.* B **72** 075407
[20] Dil J H, Hülsen B, Kampen T U, Kratzer P and Horn K 2010 *J. Phys.: Condens. Matter* **22** 135008
[21] Slomski B, Meier F, Osterwalder J and Dil J H 2011 *Phys. Rev.* B **83** 035409
[22] Nagamura N, Matsuda I, Miyata N, Hirahara T, Hasegawa S and Uchihashi T 2006 *Phys. Rev. Lett.* **96** 256801
[23] Moras P, Theis W, Ferrari L, Gardonio S, Fujii J, Horn K and Carbone C 2006 *Phys. Rev. Lett.* **96** 156401
[24] Meyer G and Rieder K H 1995 *Surf. Sci.* **331** 600
Horn-von Hoegen M, Schmidt T, Meyer G, Winau D and Rieder K H 1995 *Phys. Rev.* B **52** 10764
Smith A R, Chao K-J, Niu Q and Shih C-K 1996 *Science* **273** 226
Paggel J J, Miller T and Chiang T-C 1999 *Science* **283** 1709
Budde K, Abram E, Yeh V and Tringides M C 2000 *Phys. Rev.* B **61** 10602
Aballe L, Rogero C, Kratzer P, Gokhale S and Horn K 2001 *Phys. Rev. Lett.* **87** 156801
Aballe L, Rogero C and Horn K 2002 *Phys. Rev.* B **65** 12531
Miyazaki M and Hirayama H 2008 *Surf. Sci.* **602** 276
[25] Vosko S H, Wilk L and Nusair M 1980 *Can. J. Phys.* **58** 1200
[26] For a program description, see www.flapw.de
[27] Holst B, Nohlen M, Wandelt K and Allison W 1998 *Phys. Rev.* B **58** R10195
[28] Brune H, Giovannini M, Bromann K and Kern K 1998 *Nature* **394** 451
[29] Yeh J J and Lindau I 1985 *At. Data Nucl. Data Tables* **32** 1
[30] Ashcroft N W and Mermin N D 1987 *Solid State Physics* (Philadelphia, PA: Saunders)
[31] Moras P, Wortmann D, Bihlmayer G, Ferrari L, Alejandro G, Zhou P H, Topwal D, Sheverdyaeva P M, Blügel S and Carbone C 2010 *Phys. Rev.* B **82** 155427
[32] Wessendorf M, Wiemann C, Bauer M, Aeschlimann M, Schneider M A, Brune H and Kern K 2004 *Appl. Phys.* A **78** 183
[33] Paniago R, Matzdorf R, Meister G and Goldmann A 1995 *Surf. Sci.* **331–333** 1233
Paniago R, Matzdorf R, Meister G and Goldmann A 1995 *Surf. Sci.* **336** 113